Magnetic sensing for microstructural assessment of power station steels: Magnetic Barkhausen noise and minor loop measurements

Magnetic sensing for microstructural assessment of power station steels: Magnetic Barkhausen noise and minor loop measurements

JW Wilson[1*], N Karimian[1], W Yin[1], J Liu[2], CL Davis[2], AJ Peyton[1]
[1]School of Electrical and Electronic Engineering, University of Manchester, Manchester M60 1QD, UK
[2]School of Metallurgy and Materials, University of Birmingham, Edgbaston, Birmingham B15 2TT, UK

Abstract. There are currently no techniques available to monitor the microstructural condition of power station steel components in-service (at elevated temperatures). Electromagnetic (EM) inspection methods have the potential to provide a solution to this problem. Tests have been carried out on power generation steel (P9 and T22) samples with different microstructural states using major and minor B-H loop measurements and correlations established between EM properties and material properties such as Vickers hardness. These correlations will be used to develop a field deployable tool for the quantification of degradation in power station steels.

1. Introduction

Current procedures for the assessment of the condition of components in power stations involve site inspections during costly shut-down periods and inspection of steel components often involves lengthy procedures such as replica metallography [1, 2]. The use of electromagnetic (EM) sensors for inspection has the potential to provide information on microstructural changes in steel by exploiting the link between the microstructure and magnetic domain structure of the material. EM inspection [3-5] has the advantage that it can be performed in-situ, at elevated temperatures, with minimal surface preparation.

In this paper, the results of tests carried out on EM characterisation of power station steels are provided. Section 2 details the equipment constructed for the tests and gives an overview of the steel samples. The experimental results are provided in section 3, including; Magnetic Barkhausen Noise (MBN) with major *B-H* loop excitation; the derivation of incremental permeability curves using minor *B-H* loop excitation and MBN measurement with minor loop excitation. The paper concludes with a discussion and comparison of the results.

2. Measurement System and Sample Summary

2.1. Measurement system

A schematic of the measurement system developed for the tests is shown in figure 1. A low frequency time varying signal is fed to two power amplifiers, which supply current to two excitation coils wrapped around a silicon-steel core. The cylindrical sample is fitted into a slot in the core, to maximise coupling between core and sample. The axial applied field (*H*) is measured using a Quantum Well Hall sensor, developed at the University of Manchester. The flux density of the induced field (*B*) is measured using a 20-turn encircling coil connected to an instrumentation amplifier. For MBN

* John.Wilson@manchester.ac.uk

measurements, the 20-turn coil is replaced with a 6000-turn encircling coil and the low frequency component of the signal is rejected through the addition of a passive 5 kHz high-pass filter.

For the major loops, 1 Hz sinusoidal excitation is used and 9 cycles are recorded and averaged. A 10 Hz sinusoidal excitation is used to generate the minor loops, with two types of minor loop being recorded; 1) Deviations from the main *B-H* loop. In this case, the sample is taken through several major loop cycles before the applied field is held constant at a pre-determined *H* value and several minor loop cycles are recorded; 2) Deviations from the initial magnetisation curve. The sample is demagnetised by the application of 10 Hz sinusoidal excitation, gradually reducing in amplitude. The applied field is then increased to a pre-determined *H* value and several minor loop cycles recorded. For both types of minor loop, up to 90 cycles are acquired and averaged, to reduce noise.

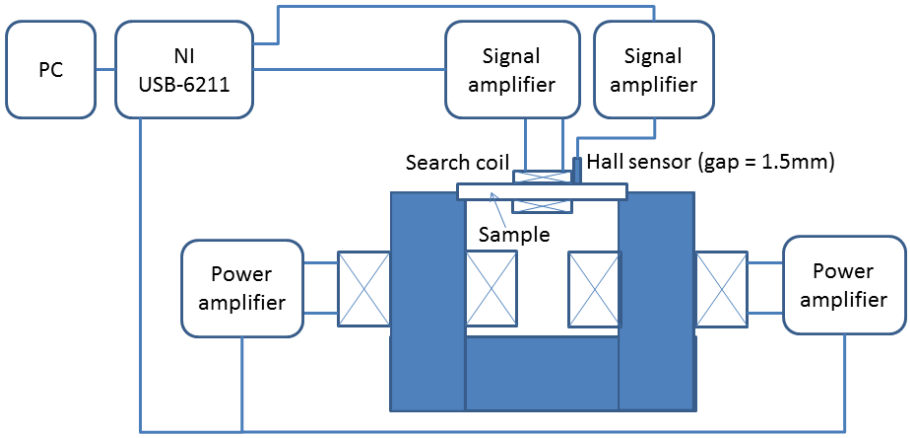

Figure 1. Schematic of measurement apparatus

The 1 Hz sinusoidal excitation is used to generate major loop MBN profiles, with the signal from the MBN pickup coil and the applied axial field from the Hall sensor recorded simultaneously. The signal from the coil is then high-pass filtered at a frequency of 5 kHz, rectified, and a moving average technique used to generate the MBN profile, which is then plotted against H. A similar process is used for the minor loop MBN readings, with the minor loop generated as outlined above.

2.2. Test Samples

Two sample sets have been studied, consisting of three P9 samples and three T22 samples. The P9 samples were machined from material which was in service for approximately eleven years at 520°C. Samples were heat treated to simulate service entry microstructure by normalising and tempering, as normalised samples were also assessed. Heat treatments, composition details and Vickers Hardness numbers (HV) are given in Table 1. Cylindrical rods with a diameter of 4.92±0.03 mm and a length of 49.59±0.54 mm were removed from the samples at each stage to create taken-from-service, tempered (and normalised), and normalised samples for both materials.

Table 1. Sample composition (in wt%), heat treatments and Vickers harness number (HV)

	P9					**T22**				
	Cr	**Mo**	**C**	**Si**	**Mn**	**Cr**	**Mo**	**C**	**Si**	**Mn**
%	8.4	0.97	0.12	0.52	0.44	1.90-2.60	0.87-1.13	0.05-0.15	0.5 (max)	0.30-0.60
	P9-TEMP		**P9-TFS**		**P9-NORM**	**T22-TEMP**		**T22-TFS**		**T22-NORM**
	Tempered at 760°C for 1h		Taken from service		Normalised at 950°C for 1h	Tempered at 760°C for 1h		Taken from service		Normalised at 950°C for 1h
HV	212		158		401	203		129		316

Complete metallographic tests were carried out at each stage; micrographs for the tests have been presented previously [3, 4]. The microstructure of the as-normalised P9 consists of predominantly martensite mixed with some bainite. Subsequent tempering produces a simulated service entry

microstructure, i.e. tempered martensite / bainite. After long service exposure, the microstructure showed equiaxed ferrite with large carbides distributed within ferrite grains or on grain boundaries.

The as-normalised T22 steel shows a mixed microstructure of bainite and some proeutectoid ferrite. No carbides are present in the ferrite, but plate-like carbides can be seen within the bainite region. After tempering, many carbides can be observed along prior austenite grain boundaries, on ferrite boundaries or within bainite regions. The microstructure of T22 after service exposure consists of equiaxed ferrite and a great many carbides outlining the ferrite grain boundaries or finely dispersed within the ferrite grains.

The HV values follow the same trend for each sample set; lowest for the taken-from service sample and highest for the normalised sample. As P9-NORM is predominantly martensitic, it exhibits the greatest HV value. As bainite typically has a lower hardness than as-quenched martensite, but higher hardness than ferrite, the bainite / proeutectoid ferrite microstructure of T22-NORM shows a reduction in HV in comparison to P9-NORM. The decrease in hardness for service exposure is reflected by a decrease in HV for both sample sets.

3. Measurement and experimental results

3.1. Major B-H Loop and MBN Measurements

Figure 2 shows major *B-H* loops for both sample sets and corresponding MBN profiles (only the profile corresponding to half of the magnetisation cycle is shown for clarity). Examination of the coercivity (H_C), remanence (B_R) and MBN peak (MBN_{PK}) values in comparison to HV shows that H_C exhibits the strongest correlation with hardness, though the decrease in H_C for service exposure is relatively small. It can be seen from figure 2 that the MBN peak position also follows the trend in H_C.

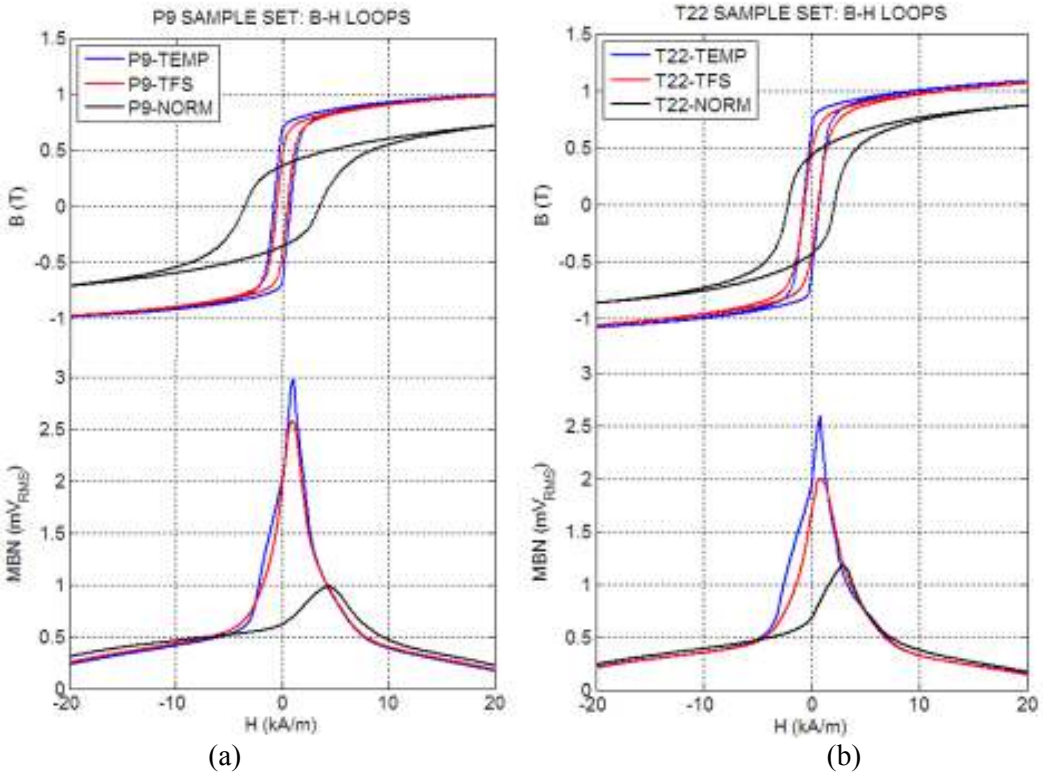

(a) (b)

Figure 2. *B-H* loops and corresponding MBN profiles for a) P9 samples, b) T22 samples

3.2. Minor Loop Measurements

The evolution of the minor loop as deviations from the initial magnetisation curve is shown in figure 3. The origin of the first minor loop corresponds to the demagnetised state (*B=0, H=0*). In this state, for a small applied field (*H*), the magnetisation (*M*) of the material can be described by Raleigh Law [6]:

$$M = \chi_0 H + \alpha_R \mu_0 H^2 \quad (1)$$

Where χ_0 is initial susceptibility, describing the reversible part of magnetisation, the Rayleigh constant α_R describes the irreversible Barkhausen jumps and μ_0 is the permeability of free space. Thus, in this region, magnetisation is a combination of reversible and irreversible components, resulting in a loop enclosing a relatively large area, as show in figure 3 (bottom left). As the initial magnetisation curve approaches saturation, domain walls are swept away by field pressure and the dominant magnetisation mechanism is the progressive alignment of the field against anisotropy [6]. Thus, only reversible components remain, resulting in a loop with a much smaller area, with a smaller ΔB for a given ΔH, as shown in figure 3 (bottom right).

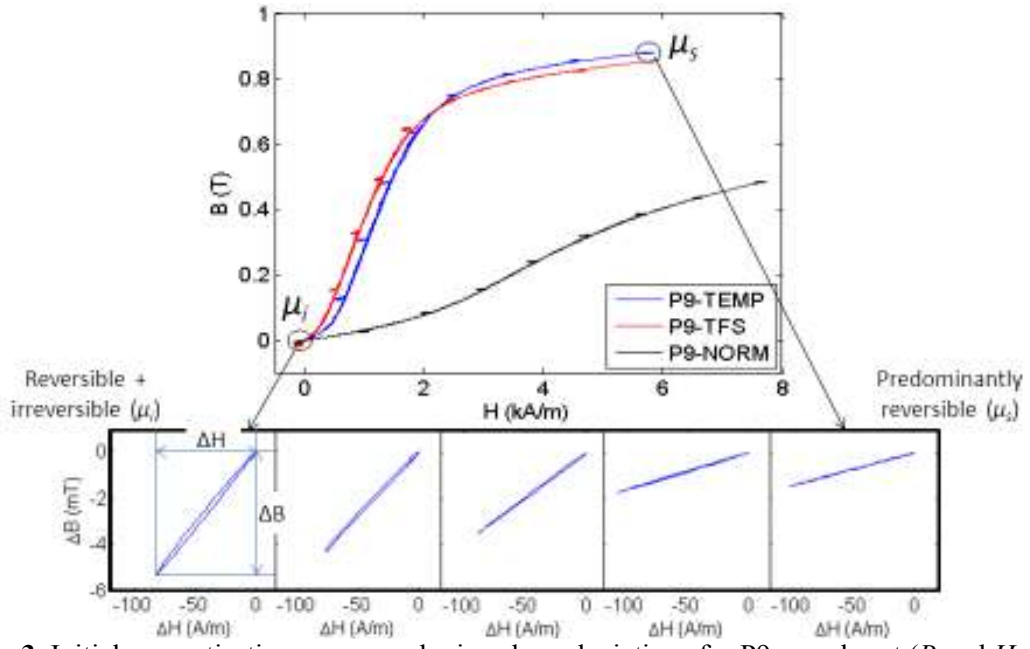

Figure 3. Initial magnetisation curves and minor loop deviations for P9 sample set (*B* and *H* offsets removed from minor loops for comparison)

Incremental permeability (μ_Δ) is calculated as the ratio between the change in flux density (ΔB) and the change in the applied field (ΔH) scaled with respect to the permeability of free space (μ_0); $\mu_\Delta = \Delta B/\Delta H\mu_0$. Figure 4a shows the resultant incremental permeability curves for minor loop deviations from the initial magnetisation curve. It can be seen from the plot that the maximum permeability values for the initial magnetisation curves correspond to the initial permeability (μ_i) reading; the point at which domains have the greatest degree of freedom to overcome pinning sites, resulting in the greatest change in *B* for a given applied field. There is a sharp decrease in μ_Δ with increasing *H* and some convergence in μ_Δ values for the three samples as saturation is approached and contributions from domain wall pinning sites are reduced, giving way to reversible domain rotation effects. P9-NORM exhibits a much smaller variation in μ_Δ for increasing *H*, as the high dislocation density of the predominantly martensitic sample results in heavy domain wall pinning and irreversible magnetisation effects are minimised. Figure 4b shows the μ_Δ curves for minor loop deviations from the major *B-H* loop. It can be seen from the plot that the maximum μ_Δ value ($\mu_{\Delta\text{-}max}$, table 2) corresponds to the coercive field. As with the initial curve results, this is the point at which *B=0* and domain walls have the greatest degree of freedom to move.

Figure 4c shows the P9-TEMP curves from figures 4a and 4b together for comparison. Although the curves have different values at *H=0*, they converge at H_C as the initial magnetisation curve and major *B-H* loop converge. It is apparent from the plot that the random domain structure of the demagnetised sample corresponding to the μ_i reading results in a greater variation in *B* for a given *H* field than the systematic reorganisation of domains at H_C.

As operating in the Raleigh region results in the highest permeability values and it has been found that minor loop measurements in this region are highly sensitive to lattice defects [7], the effect of

varying the amplitude of the minor loop used to calculate μ_i has been investigated. Figure 5 shows plots of μ_i for P9 and T22 for a variation in minor loop amplitude. It can be seen from the plots that as the minor loop amplitude increases, so does μ_i. At low minor loop amplitudes, reversible magnetisation dominates ($\chi_0 H$, equation (1)) as the minor loop amplitude increases, the irreversible component ($\alpha_R \mu_0 H^2$ equation (1)) is introduced and the gradient of the minor loop increases, as a greater ΔB is generated for a given change in H. Polynomial fitting has been employed to extrapolate values for μ_i if the minor loop amplitude could be made to equal zero; see $\boldsymbol{\mu}_{i\text{-}H0}$, table 2.

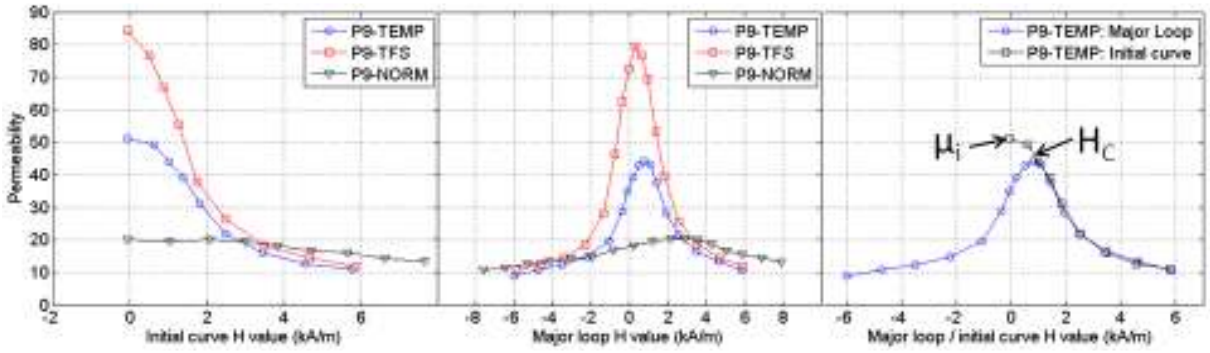

(a) (b) (c)

Figure 4. a) Incremental permeability curves for initial magnetisation, b) μ_Δ curves for major *B-H* loop, c) μ_Δ curves for initial magnetisation and major *B-H* loop for sample P9-TEMP

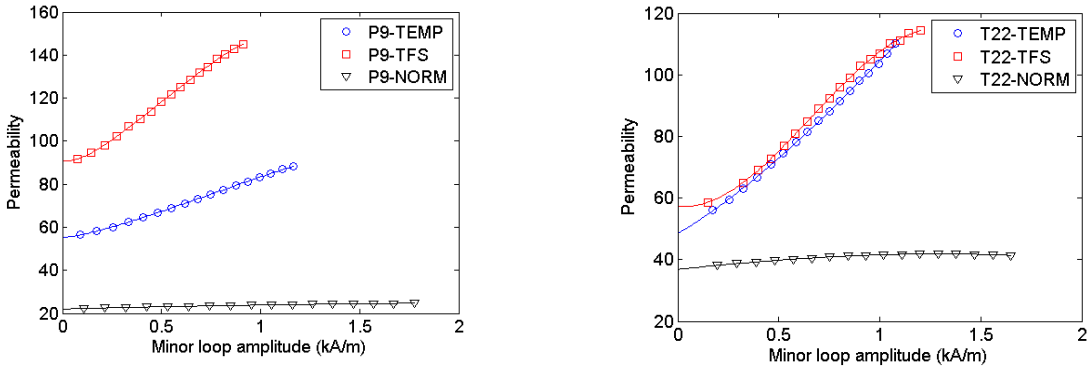

(a) (b)

Figure 5. Initial permeability (μ_i) values derived from a minor loop amplitude sweep for; a) P9 sample set b) T22 sample set

3.3. Minor Loop Magnetic Barkhausen Noise

The change in MBN_{RMS} values derived from a minor loop amplitude sweep for initial permeability is shown in figure 6a. It can be seen from the plot that at higher minor loop amplitudes, MBN_{RMS} follows a similar trend to the permeability values derived from the minor loop, as shown in figure 5a; with the MBN value for the P9 ex-service sample increasing rapidly and reaching the highest amplitude, increasing less rapidly for the tempered sample and exhibiting very little change for the normalised sample. However, at lower amplitudes the plots for the three samples converge, only showing a significant increase in amplitude at around 0.3 kA/m for P9-TFS and 0.5 kA/m for P9-TEMP. This indicates that only at these higher applied fields do the domain walls gain enough energy to overcome particular pinning sites in the material.

The plots for the T22 samples (figure 6b) exhibit a similar trend. However in contrast with the results for P9, T22-TFS and T22-TEMP start to cross over, reflecting the fact that tempered samples give the highest level of MBN for major loop excitation (see figure 2). It is also notable that the point at which the samples exhibit a significant increase in amplitude is indicative of the trend in H_C.

In order to provide a single minor loop MBN reading for each sample ($MBN_{\mu i}$, table 2), it was decided to choose the readings at the point where the minor loop amplitude reaches the coercive field value for P9-TEMP and T22-TEMP for the P9 and T22 sample sets respectively. This point was

chosen because the tempered samples represent the service entry microstructure of the two steels, therefore the H_C values represent a fundamental magnetic property of these steels.

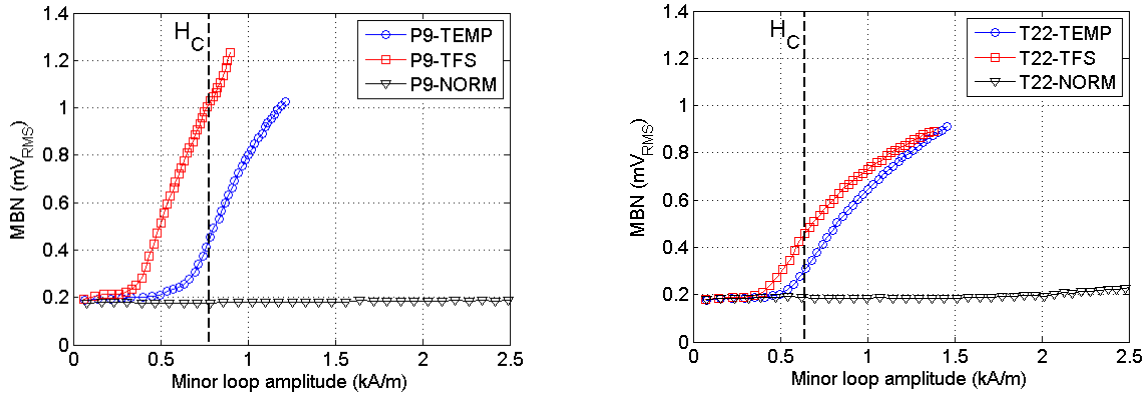

Figure 6. MBN_{RMS} values derived from initial permeability (μ_i) minor loop amplitude sweep for; a) P9 sample set b) T22 sample set

4. Discussion and Conclusions

Table 2 shows the various signal features collected from the tests in this paper. All the minor loop features ($\mu_{i\text{-}H0}$, $\mu_{\Delta\text{-}max}$, $MBN_{\mu i}$) have an inverse relationship with HV, increasing from normalised to tempered to taken-from-service. Although H_C is not directly proportional to HV, it does follow the same trend, though the change in H_C for service exposure is much smaller than for the minor loop parameters, indicating that the minor loop features may be more sensitive to changes in microstructure due to service exposure.

Table 2. Major loop, permeability and MBN values

	P9-TEMP	P9-TFS	P9-NORM	T22-TEMP	T22-TFS	T22-NORM
HV	212	158	401	203	129	316
B_R **(T)**	0.68	0.44	0.36	0.63	0.46	0.43
MBN_{PK} **(mV$_{rms}$)**	2.98	2.58	0.98	2.59	1.10	1.18
H_C **(kA/m)**	0.78	0.51	3.51	0.72	0.64	2.15
$\mu_{i\text{-}H0}$	55.2	90.9	22.0	48.5	57.4	36.9
$\mu_{\Delta\text{-}max}$	44.3	79.6	20.3	38.6	51.5	35.2
$MBN_{\mu i}$ **(mV$_{rms}$)**	0.46	1.03	0.18	0.31	0.46	0.19

This work shows that there are clear relationships between EM features and microstructural changes in power station steels. Although major *B-H* loop features are useful, this type of measurement is difficult to achieve on open samples (i.e. pipes and tubes). MBN and permeability readings derived from minor loops are easier on open samples, require less power, and by looking at the change in readings rather than absolute values, may not require an accurate *H* field measurement; as *H* is heavily dependent on geometry. The next step of this work will be to exploit the correlations established using closed magnetic loop tests to develop a tool for the inspection of pipes and tubes in power stations.

References

[1] Maharaj C, Dear JP, and Morris A 2009 *Strain* **45(4)** 316-331
[2] Sposito G, Ward C, Cawley P, Nagy PB and Scruby C 2010 *NDT & E Int.* **43(7)** 555-567
[3] Liu J, Hao XJ, Zhou L, Strangwood M, Davis CL, Peyton AJ, 2012 *Scripta Materialia* **66** 367–370
[4] Yin W, Karimian N, Liu J, Hao XJ, Zhou L, Peyton AJ, Strangwood M and Davis CL 2012 *NDT & E Int.* **51** 135-141
[5] Wilson JW, Tian GY, Moorthy V and Shaw BA 2009 *IEEE Trans. Magn*. **45** 177-183
[6] Bertotti G 1998 Hysteresis in magnetism: for physicists, materials scientists, and engineers (San Diego:Academic Press)
[7] Takahashi S, Kobayashi S, Kikuchi H, and Kamada Y 2006 *J. Appl. Phys.* **100** 113-908